UNIVERSIDADE D
COIMBRA

Diogo Monteiro Martins

Simulation of Prostate Tissue and Cancer Development in 3D

Project in Biomedical Engineering lectured in the Degree in Biomedical Engineering supervised by the Professors João Carvalho and Rui Travasso and developed in the Center for Physics of the University of Coimbra at the Physics Department at the Faculty of Science and Technology of the University of Coimbra

June 2023

Contents

Introduction

The present project was developed in the scope of the Project in Biomedical Engineering course, lectured during the second semester of the third year of the Degree in Biomedical Engineering. This degree is taught at the Faculty of Science and Technology of the University of Coimbra. The project was developed in the Center for Physics of the University of Coimbra (CFisUC) at the Physics Department under the guidance of the supervisors João Carvalho and Rui Travasso.

The research topic was proposed by the supervisors with the aim of simulating a three-dimensional model of prostate tissue and cancer development through the usage of computational modeling. The current work was modeled using the programming language C/C++ and was based on a previous paper made by the supervisors (Carvalho J, et al. [1]) that modeled urothelium tissue and bladder cancer.

The project was developed through the entire semester and was structured into manageable weekly objectives to ensure steady progress. The first weeks, before the beginning of the semester, the first contact with the programming language C/C++ was done through the completion of several online courses recommend by the supervisors. At the beginning of the semester, after the first reunion in which a global explanation of the project was provided, a deep study on the prostate anatomy and histology, as well as the prostate cancer itself was performed by analyzing books and papers in this topic. Subsequent to the understanding of the prostate characteristics, a three-dimensional model to represent one acinus of the prostate glands was developed. As the project advanced, the acinus geometry was adapted and changed accordingly to the results obtained, as both cells and the overall system suffered significant changes. Upon reaching the final geometry and obtaining the adjusted parameters for the model, the systematic study of the most important elements of the adenocarcinoma growth began. The influence in the adenocarcinoma development of changing variables like the tumor starting layer, the cells' stiffness, the adhesion energy, and others, was carefully analyzed to suggest possible therapeutic targets. In the final weeks of the semester, this report was written.

Even though this project allowed to gain insights in the prostate tumor development and how to better control it, complementary work to deepen this knowledge could be done. Specifically, the implementation of some of the therapies already available for prostate adenocarcinoma treatment as well as model and suggest new ones. The creation of a more complex geometry containing several acini (possibly a whole tubuloalveolar gland) and the simulation of the different tumor stages and their effect in the prostate would also be a great improvement and would allow a comparison with the Gleason criteria. Additionally, keep track of the changes induced by the introduction of blood vessels in the model and allowing tumoral cells to have easier access to the nutrients and oxygen transported upon stromal invasion can also allow the model to take one step closer to the reality of a prostatic adenocarcinoma.

Lastly, I would like to acknowledge the availability of the supervisors João Carvalho and Rui Travasso, who have consistently demonstrated their willingness to clarify any doubts and provide explanations on the various topics discussed throughout the project.

Theoretical Fundaments

Prostate Anatomy and Histology

The prostate gland [2-5] is one of the three accessory glands that belong to the male reproductive system. It is an organ with an inverted pyramid-shape format, located in the pelvic cavity, bellow the bladder and posterior to the rectum, surrounding the prostatic portion of the urethra that transports the urine from the bladder (Figure 1A). Anatomically the prostate is divided in three different zones (Figure 1B), the central zone (represents about 25% of the prostate tissue), the transition zone (composes around 5% of the gland total volume) and the peripherical zone (represents approximately 70% of the prostate tissue).

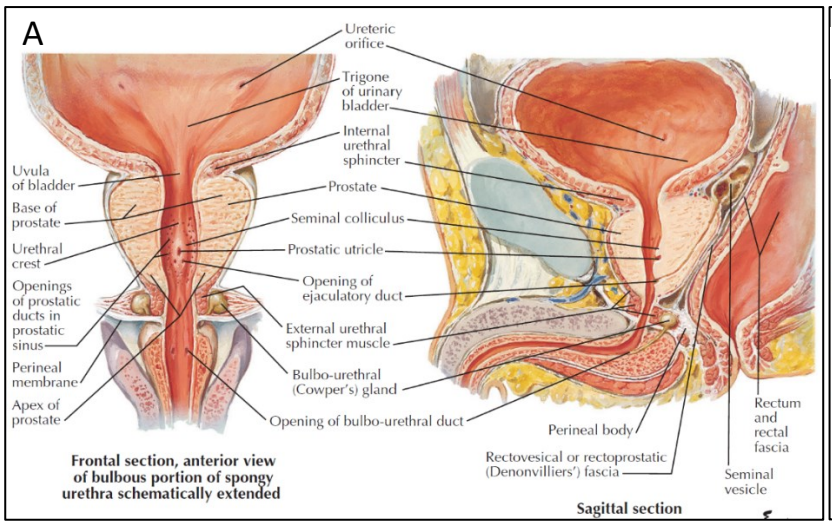

Figure 1A - Prostate Anatomy [4]

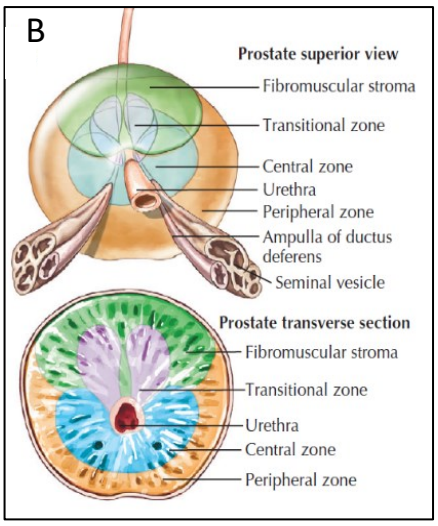

Figure 1B - Prostate Anatomic Zones [4]

Histologically [6], the prostate is comprised of 30 to 50 branched tubuloalveolar glands surrounded by a fibromuscular stroma containing smooth muscle cells, fibroblasts, blood vessels and nerves. The glandular epithelium is either cuboidal or pseudostratified columnar in shape and forms multiple acini and ducts within each gland. The epithelium is composed of three distinct cell types, the luminal, the neuroendocrine and the basal cells [7]. Luminal and neuroendocrine cells are responsible for secreting various products in the acinus lumen, while basal cells are adjacent to the basal membrane and have a support function (Figure 2).

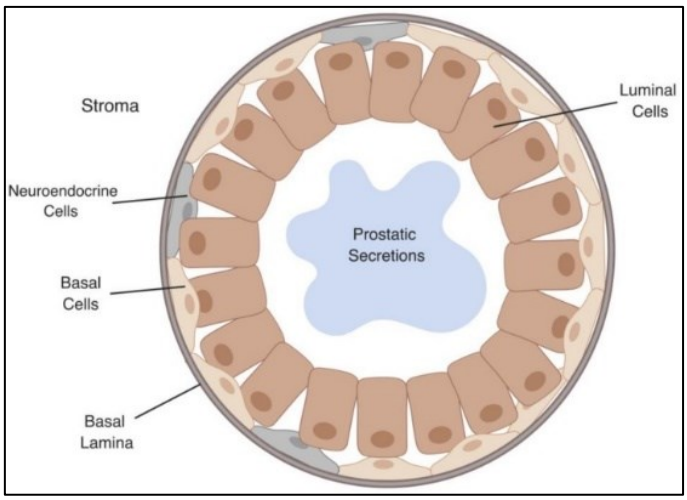

Figure 2 - Cells of the Glandular Epithelium [7]

According to the project objectives, through the observation of histological images it was possible to better understand the acinus structure and design a three-dimensional geometry to represent it. Analyzing both Figure 2 and Figure 3, it is possible to observe the cells that compose the epithelium, and with the scale in the figures attribute to each cell its respective dimension and shape. The model design included the luminal and basal cells, the lumen, and the stroma of one acinus. The neuroendocrine cells were not included in the model due to their irrelevance for this study case and to avoid further complexity. In Table 1 are given the real cell dimensions and the cell dimensions in cylindrical coordinates that were posteriorly used to create the model. The cells in the model are slightly smaller when compared to the real cells because the model domain comprehend different dimensions than those viewed in Figure 3. However, the cell proportions were maintained. The reduction of the domain dimensions is justified by the need to decrease simulation running times, while concurrently enabling enhanced control over cell parameters through the usage of smaller cells. A posterior analysis of the results needs to be done to convert from the model scale to the real scale.

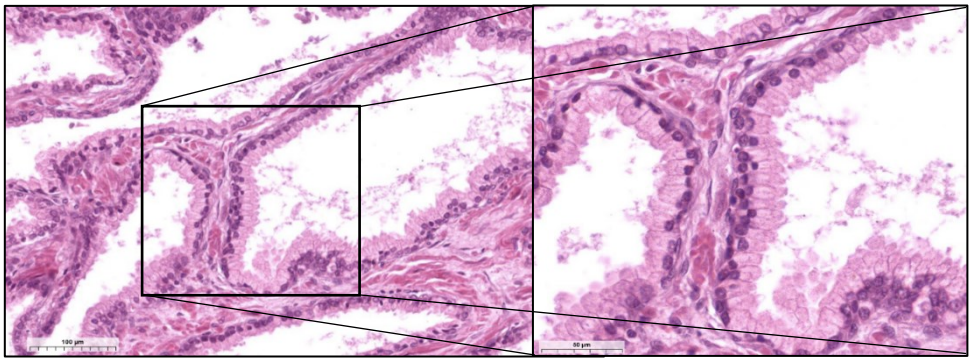

Figure 3 – Prostate Acinus Histological Image [6]

Table 1 - Real Cell Dimensions and Model Cell Dimensions

	Real (Cartesian Coordinates)			**Model (Cylindrical Coordinates)**		
Type	**Height (μm)**	**Width (μm)**	**Depth (μm)**	**ρ (μm)**	**ϕ (rad)**	**z (μm)**
Luminal Cell	8	6	20	13	0.05π	4
Basal Cell	5	5	8	5	0.05π	4
Lumen	–	200	280	91	2π	252
Stroma	–	280	340	–	2π	252

The acinus geometry was approximated to a cylinder and using the model dimensions it was possible to obtain Figure 4, which represents its top ($z = 150$) and lateral ($x = 75$) views.

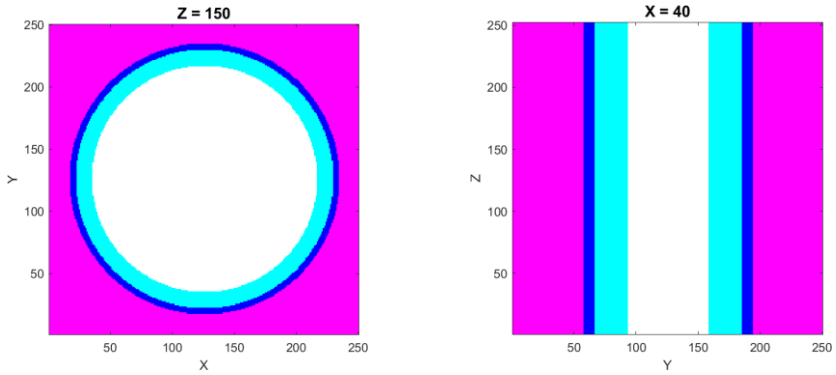

Figure 4 – Acinus Top (Left) and Lateral (Right) Views

In Figure 4 it is possible to observe four different colors as each one represents a different cell type used in the model. The colors pink, dark blue, light blue and white correspond to the stroma, basal cells, luminal cells, and lumen, respectively. The tumoral cells, which will be introduced later on the model, are represented by a grey tone (observed in Figure 10).

Prostate Cancer

Prostate Cancer [9] is the second most prevalent cancer in male individuals. In 2018 around 1.2 million new cases of prostate cancer were diagnosed worldwide, resulting in approximately 360.000 deaths, according to the Global Cancer Observatory (GCO). The average annual incidence of new diagnostics for this disease is around 190.000 with approximately 80.000 registered deaths globally. The GCO projections suggest that due to the exponential growth of the world population and the increasing number of male individuals aged 65 and older, the number of new prostate cancer cases will approach 1.7 million by the year of 2030, and mortality rates may surpass the half a million mark.

Prostate cancer, like many other diseases, is influenced by several causative risk factors [9]. These factors can be classified in two categories, the modifiable and the non-modifiable. Modifiable risk factors, such as smoking, can be altered by individuals, while non-modifiable risk factors, such as age and genetic predisposition are beyond the individual's control. Genetics represent the most relevant risk factor for the development of prostate cancer. Males whose relatives have previously been diagnosed with cancer (not necessarily prostate cancer) have a 50% higher chance of developing the disease. Black men are also more likely to be diagnosed with prostate cancer due to their high predisposition to certain types of genetical mutations. Age is also a significant factor, considering that the probability of being diagnosed with prostate cancer increases exponentially after the age of 50. However, the chances of being diagnosed for individuals under the age of 40 are very low. Other risk factors include diet, weight, smoking and exposure to certain chemical agents.

Prostate cancer is extremely complex regarding all the biological agents and mutations that have a relevant role in its development. Depending on the tumor progress and the changes on the healthy tissues, four stages (Figure 5) can be distinguished until it reaches the full development [9]. In a very simplified way, the first stage of prostate cancer is an inflammation of the prostate gland due to uncontrolled cell proliferation (caused by a DNA mutation). This stage is called prostatic intraepithelial neoplasia (PIN) and is not yet a cancerous condition. The tumor then advances into a localized prostate adenocarcinoma (latent) where the lumen is invaded by tumor cells. The next stage is prostate adenocarcinoma with local invasion (clinical), implying that the basal cell layer is degraded allowing the tumor to proliferate to the lamina propria. The last stage is metastatic prostate cancer where the tumor invades and proliferates in other tissues. Firstly, the lymph nodes adjacent to the tumor initial site are metastasized and then, through the bloodstream and the lymphatic system, other organs, including bones, liver and lungs, also suffer metastasis.

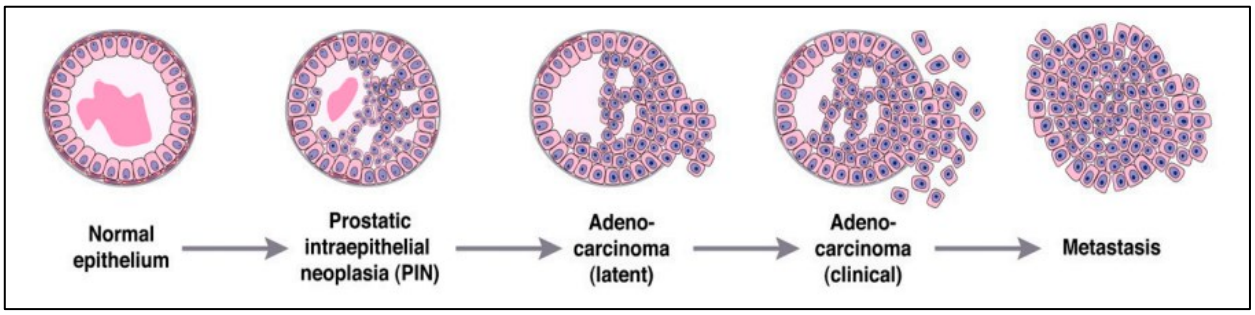

Figure 5 - Progression of Prostate Cancer [9]

Current research investigates the impact of the initial tissue in prostate tumor growth and if this factor affects in any way the possible outcome [11]. It has already been established that the likelihood of developing prostate adenocarcinoma differs across the different anatomical tissues [3]. Specifically, the central, transition and peripherical zones have probabilities of 5%, 25% and 70%, respectively. Both the cells of the luminal and basal layers can suffer mutations and cause tumor growth [11], but the studies regarding the biological and clinical relevance of each case have not yet reached a consensus about a possible influence on the prognosis. Furthermore, it remains unknown whether the neuroendocrine cells can undergo mutations making them prone to generate prostate adenocarcinoma.

Finally, it is still important to understand how to diagnose and the possible therapies available for prostate adenocarcinoma. The three principal tests done [9] are the digital rectal examination (DRE), the prostate-specific antigen test (PSA) and biopsies. The DRE test gives a better understanding of the size of the gland and any abnormalities, while the PSA test is based on the analysis of blood samples to determine the quantity of PSA (glycoprotein secreted by epithelial cells of the gland). The second diagnosis is the most used, although high levels of PSA in the bloodstream may not indicate a malign pathology as patients with benign prostatic hyperplasia also have increased levels of PSA. A biopsy is a medical procedure in which a tissue sample is removed from the prostate gland to be observed and studied under a microscope. It is usually supplemented with imaging by devices such as magnetic resonances and transrectal ultrasounds, allowing the clinician to target specific areas of the prostate. Even though the biopsy represents an invasive procedure it produces the most reliable results. Radical prostatectomy, even though it is a treatment procedure (that will be discussed later), can also be used to perform a disease diagnosis. The prognosis is based on the results of these tests merged with the conclusions withdrew from the Gleason grading system.

The Gleason system [12-14] has been upgraded throughout the years, based on new insights and experiments. The most recent version was approved in 2014 at the International Society of Urological Pathology Consensus Conference and consists in a five-grade group system based on the Gleason score from 1 to 10 (already revised in 2005), that considers different types of prostate adenocarcinoma growth patterns [15]. The Gleason score is determined in different ways when a biopsy or a radical prostatectomy is performed. In the biopsy case, the score is determined through the addition of the highest grade and the most common grade found in the tissue. Considering the radical prostatectomy, the Gleason score is obtained by adding the two most predominant grades found when analyzing the prostate tissue. The first group includes all prostate cancers with a Gleason score of 6 or lower associated with low risk and little to no disruption of the glandular tissue. The second group was assigned to the score of 7 in the Gleason system and most of the tissue is composed of well-formed glands, while some glands have differences in terms of their shape (poorly formed, fused, glomeruloid, or cribriform glands). Regarding the third group, the Gleason score associated with it is still 7. However, in this case there is a predominance of poorly formed, fused, glomeruloid, or cribriform glands when compared to the number of glands with a well-formed shape. The fourth group comprises the 8 score of the Gleason criteria and is characterized by three distinct scenarios. In the first one, the tissue is only composed of poorly formed, fused, glomeruloid, or cribriform glands. In the second one well-formed glands are predominant, and a small portion of the tissue lacks any type of gland. In the last case, most of the tissue is lacking any type of gland and only a minor portion is composed of well-formed glands. Finally, the fifth group includes the scores 9 and 10 of the Gleason system and is described by a small number of glands poorly formed, fused, glomeruloid, or cribriform and the lack of glands on the remaining tissue, or, in the worst case, a complete lack of glands. There are studies that fundament that different three-dimensional architectures of prostate cancer growth patterns lead to different prognostic, and can be used to assign personalized risk and possible treatments. Studies around this issue are still being conducted to better understand how these differences can be beneficially used. Thanks to the endless improvements in long distance confocal laser scanning, tissue-clearing techniques and light-sheet microscopy, it is already

possible to create three-dimensional models of prostate tissues that correspond to the Gleason patterns observed (Figure 6).

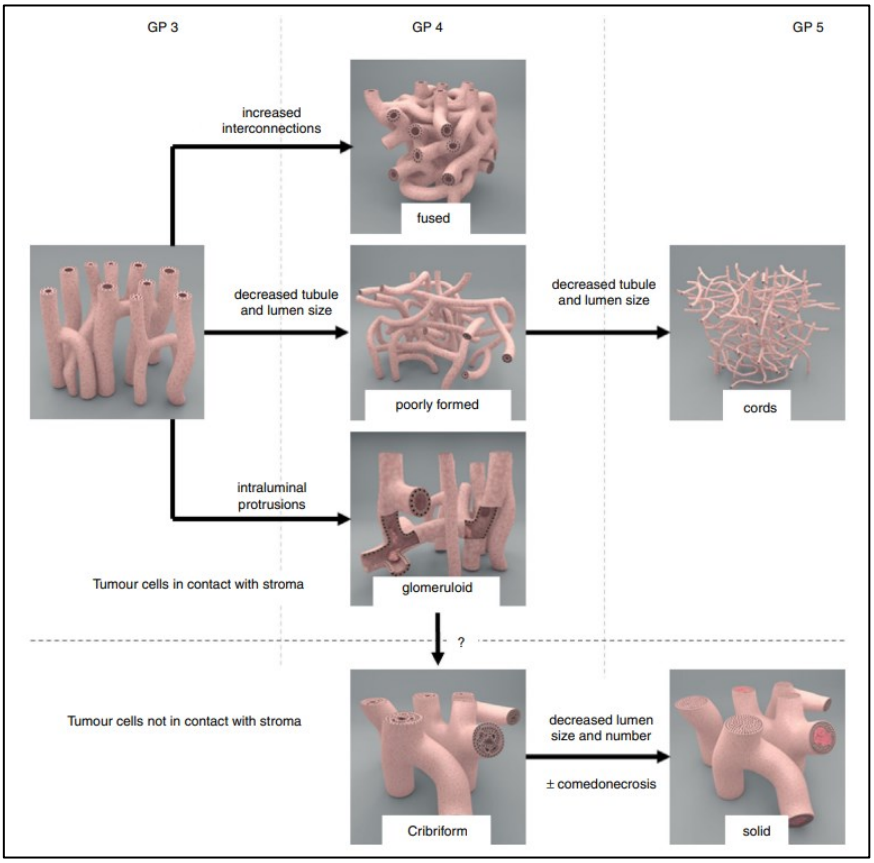

Figure 6 – Three-Dimensional Tumor Growth Patterns [15]

Prostate Cancer Treatment

Following the confirmation of the prostate adenocarcinoma diagnose, a wide spectrum of treatment possibilities can be considered [9,16]. The selected option will depend on the risk category (stage of the cancer) and the prognosis made. Men whose clinical risk is low or, in some cases, intermediate, will be mostly recommended for active surveillance. The other cases of intermediate risk may decide to undertake a more invasive path through ablative therapies, radical prostatectomy, or radiation therapy. Individuals diagnosed with local invasion or metastatic adenocarcinoma are recommended to proceed with radiation therapy with a possible aid of hormonal therapy. In the most severe cases, where the tumor is already in a metastatic stage and has shown resistance to the previous types of therapies, the possibility of chemotherapy treatment is offered. Active surveillance is a program designed to accompany the patient and monitor its disease evolution. Ablative therapies use the incidence of energy in the prostate to eliminate the tumor and try to cause the least possible damage to the surrounding tissues (case of cryotherapy). Radical prostatectomy is a medical procedure that consists in removing the prostate gland through surgery, and is recommended in cases where the ablation therapy did not produce results and metastases are absent. Radiation therapy is one of the most effective ways to eliminate the tumor and can be delivered as brachytherapy or external beam therapy. Hormonal therapy, also known as androgen deprivation therapy, is based on the maximum androgen blockage leading to the stoppage of male hormones production and preventing the continuous growth of the cancerous cells. As a last resource, chemotherapy can be considered and its mechanism uses anticancer drugs to kill or prevent posterior growth of the tumoral cells. The most common drug used for prostate cancer is docetaxel. Each type of treatment has associated adverse consequences that depend on the grade of invasion

and the eliminated tissue. Some side effects may be erectile disfunction, urinary incontinence, anemia, hypersensitive reaction, and many others.

Computational Model

The current work is based on the premise that the use of computational power to model complex biological processes [17,18], allows not only to verify existing knowledge, but also to gain new insights into the behavior and underlaying mechanisms of these processes. The project focusses on applying these modelling methods to a prostate tumor, to predict different outcomes depending on several parameters and conditions that affect the tumor development. From the results acquired it is possible to envision new therapies as well as new diagnose methods and the effect of medical procedures and drugs. To model a tumor one of two approaches can be followed, namely stochastic, or analytical methods. A stochastic approach focuses on the usage of random numbers and probability distributions to simulate the evolution of a tissue environment according to a set of parameters and conditions. On the other hand, an analytical method is based on a set of complex ordinary differential equations (ODE system) that have a relation described by multiple parameters. The stochastic approach has the advantage of being able to mimic the complex nature of a tissue (which includes cell to cell communication, interaction, and proliferation dynamics), when compared to analytical methods, since these processes may pose a challenge to capture with ODE-based models. For these reasons, the stochastic approach is ideal for this project as the analytical model could possibly pose some limitations.

Computational based tumor models (*in silico*), like every other computational model, have some advantages and disadvantages when compared to *in vivo* experiments. Some of the pros of *in silico* models are the quickness of the simulation processes, the costs involved are significantly lower and they can help reduce the risks associated with the test of new treatments or interventions on living organisms (exploring different scenarios *in silico* can allow the detection of potential issues and limitations before the clinic tests are performed). However, a few cons of *in silico* simulations are the difficulty (or in some cases the impossibility) to model all biological processes due to their high complexity or even the absence of knowledge about all the processes/parameters involved, and the fact that the results of an *in silico* model always need to be validated by *in vivo* experiments.

In this project the developed 3D model is based on a stochastic approach, the Cellular Potts Model (CPM), and describes in a reasonably realistic way a tumor growth in the prostatic glands. The CPM [19-22] is a grid or lattice-based representation of the biological space (with a spatial resolution beyond the cellular level) that implements an energy minimization principle and simulates the collective behavior of interacting cells. Various cell biophysical properties that play key roles in cancer development, such as proliferation, mobility, and adhesion, are considered in these models, making them optimal for modelling these types of biological processes. The lattice is divided into equally sized voxels which can either be part of a cell or the surrounding medium. This spatial division allows for high resolution simulations; however, it implies that the cells themselves are represented as structureless entities. Essentially, each cell is treated as a collection of voxels that share certain properties and behaviors, opposite to a real cell structure where distinct organelles are present. The biological dynamics are simulated by the movement or changes in size of a cell when it annexes a voxel or when a voxel is lost and annexed by an adjacent cell.

In the CPM each voxel is assigned with an integer value, $\eta(x)$, called cell index or cell tag (like the spin value in physics), that ranges from 0 to N with unitary intervals. The 0 tag corresponds to the medium (absence of cells that can be originated by cell movement or death), while every other index from 1 to N corresponds to a certain cell (meaning that N is the total number of cells in the system). Hence, each cell is formed by the group of adjacent voxels with the same cell index. Every cell is also associated with a certain

cell type (τ) that will define its properties (namely target volume, target surface length), and how the interaction with other cells occurs (adhesion energy for example) (Figure 7).

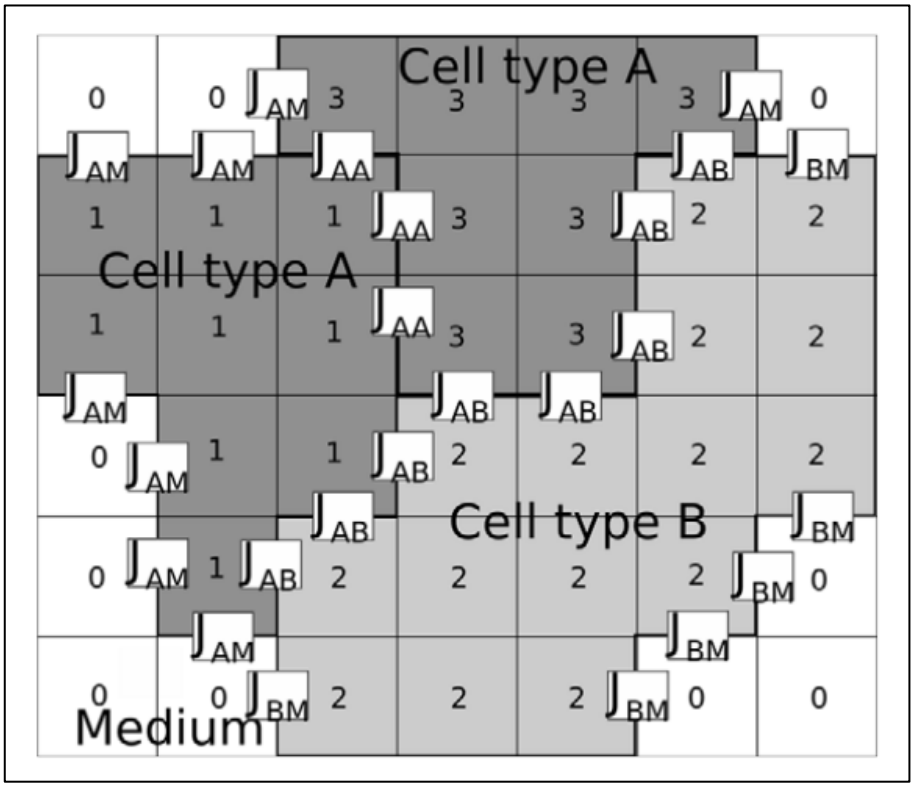

Figure 7 – CPM – Division in Cell Types and Voxels Indexes and Application of the Adhesion Energy Parameter considering the Interaction between Cells [20]

A CPM is a time-discrete Markov chain that uses the Metropolis algorithm for Monte Carlo dynamics to describe the cell's movement. This algorithm attempts to copy the cell index from one voxel to another one adjacent in an iterative and random way, based on probabilities given by the minimization of the system global energy (Hamiltonian). Each step of the model, a Monte Carlo Step (MCS), consists in trying to process these copy attempts as many times as there are voxels in the considered lattice domain. A posterior analysis of the results needs to be performed to determine how much real time corresponds to a MCS. To perform each copy, a set of rules must be followed, starting by randomly choosing a voxel (the source voxel) and one of its neighbors (the target voxel). In a 3D model, the random neighbor is chosen considering a von Neumann Neighborhood that includes 6 neighbors (result of moving one unit in each direction x, y, and z). After the selection of the voxels, the Hamiltonian difference between the current state and the future state voxel is calculated, and based on the final energy, the copy may or may not occur. The Hamiltonian, H, is an energy function that can have a dependency in numerous parameters such as the adhesion, volume, surface length and others depending on the results pretended. For this specific case (based on the Hamiltonian presented in Carvalho J, et al. [1]), the parameters that will be considered are the adhesion energy and the deviation from the target volume, resulting in the following equation for the Hamiltonian:

$$H = H_{Adhesion} + H_{Volume} = \sum_{\langle i,j \rangle} J_{\tau(\sigma(i))\tau(\sigma(j))}\left(1 - \delta_{\sigma(i)\sigma(j)}\right) + \sum_{\sigma=1}^{N} \lambda_V(\tau(\sigma))\left(\frac{V(\sigma) - V^T_{\tau(\sigma)}}{V^T_{\tau(\sigma)}}\right)^2$$

$$\Delta H = H_{(after\ copy)} - H_{(before\ copy)}$$

In the previous expression $J_{\tau\tau}$, represents the adhesion energy between two voxels of type τ and τ', and the summation over $\langle i,j \rangle$ represents the ponderation of this parameter for all the von Neumann

Neighborhood voxels (j) of the target voxel (i). Regarding the volume energy, the λ_V parameter is a penalty value for the deviation from the target volume (simulates an inelasticity constant). The values of $V(\sigma)$ and $V^T_{\tau(\sigma)}$ correspond to the cell volume in that moment and the cell target volume, respectively. The $J_{\tau\tau'}$ and the λ_V parameters are given in arbitrary units, while the parameters $V(\sigma)$ and $V^T_{\tau(\sigma)}$ are given in voxels. The calculus of this energy for all the system cells is obtained by the introduction of the sum over σ.

Considering the voxel coping rules, the Hamiltonian difference is given by ΔH and the probability of a copy being executed, p, is given by the condition:

$$p = \begin{cases} 1 & ,\Delta H < 0 \\ e^{-\Delta H} & ,\Delta H \geq 0 \end{cases}$$

If the copy occurs, the cell whose source voxel belongs to gains the neighbor voxel, meaning that the cell that was composed of the neighbor voxel loses it. If the copy does not have the necessary probability to occur, the system remains unchanged, and the simulation proceeds to try the copy of another voxel.

All the cells in the model follow a behavior that leads to homeostatic equilibrium, except for the tumoral cells. These cells grow in an uncontrolled way to double their volume, applying pressure in the healthy cells of the tissue, causing their death if their volume reaches values smaller than 20% of the target volume. The tumoral cells also have a property that differentiates them from healthy cells, the ability to proliferate. Proliferation implies that a tumoral cell has reunited the conditions to divide itself into two new tumoral cells. The first condition is the cell volume needs to increase to a point where it is 150% higher than the initial target volume. However, the volume increase is a necessary but not a sufficient condition to proliferate. The tumoral cell also needs to have a certain lifetime before it can divide. The time that needs to pass before proliferation is called cell cycle duration (calculated with a Gaussian distribution around a mean value) and represents the second condition. When both these conditions are reunited, the cell divides symmetrically in two.

The project develop was based on a previous work made by the supervisors for the urothelium and bladder cancer [1] and the general CPM parameters and each cell parameters were adapted from the ones previously used, to reproduce real systems observations and dynamics (including the homeostatic equilibrium in the absence of tumoral cells). The Table 2 and Table 3 represent the general CPM parameters and the individual cell parameters, respectively, that were used in this model. The periodic conditions on the x, y and z axis were set to false (meaning that they are not observed) as they introduced unreal dynamics in the system.

Table 2 - CPM General Parameters

Parameter	**Value**
Number MCS	1000
Cell-Medium Energy Cost	$J_{i0} = 1.8$
Cell-Cell Energy Cost	$J_{ij} = 2.55(2.30)\ for\ i \neq j(i = j)$
Volume Limit for Death Pressure	$0.2 \times V^T_{\tau(\sigma)}$
Tumor Cells Proliferation Volume (Initial)	$1.5 \times V^T_{Tumoral}$
Tumor Cells Proliferation Time	$25 \pm 5\ MCS$
Tumor Initial Layer	Luminal Layer
Domain Dimensions (x, y, z)	$250 \times 250 \times 252$

Table 3 - CPM Individual Cells Parameters

Cell Type	λ_V **(Arbitrary Units)**	**Target Volume (Voxels)**
Stroma	1×10^{12}	6.354180×10^{6}
Basal Cell	2.3×10^{3}	3.4×10^{2}
Luminal Cell	1.9×10^{3}	7.95×10^{2}
Lumen	1.7×10^{3}	6.548220×10^{6}
Tumoral	8.8×10^{3}	7.95×10^{2}

Simulation and Results Analysis

The code used to develop the model and to run the simulations was written in the programming language C/C++ and was based on the previous supervisors' code made for bladder cancer. The model standard parameters are the ones presented on Table 1 and Table 2. A comprehensive investigation of the crucial parameters, such as the inelasticity constants and the adhesion energy, was carried out by systematically varying them in an incremental or decremental way or, in some cases, by applying both changes simultaneously. For each set of specific conditions, six simulations were run, and the resulting data was analyzed using MATLAB code. The obtained results, which subsequently underwent a critical analysis, comprise various types of graphs and three-dimensional plots. The results are the two-dimensional slices of the acinus domain in accordance with different coordinates (similar to Figure 4), the tumor's three-dimensional morphology (facilitating the observation of its' volume size and shape) and some overall characteristics of the model's (mean and respective standard deviations of six simulations). The model characteristics analyzed were the tumoral, luminal and basal cell number, the tumor volume and the tumor surface area.

The introduction of the tumoral cell in the computational model was achieved through the replacement of a healthy cell, either luminal or basal, located in the left portion of the x-axis and at the midpoint of the z and y axes. To reduce the duration of each MCS, the voxels copies were performed exclusively for the left part of the x-axis domain, where the x coordinate was smaller than 100. This means that while the source voxel could be chosen from the entire domain, the copy will only be attempted if the source voxel's x-index was less than 100. Despite this change in the dynamics, the overall system morphology remained unaffected, as the tumoral cell position on the left side of the x-axis meant that the right side of the axis was only involved in the dynamic equilibrium (homeostasis) and not in the tumor growth. This change in how the voxels copies are executed allowed to reduce the duration of each MCS to about one third of its initial value, a significant decrease considering the number of simulations that needed to be run and the time limit to complete the project.

Homeostatic Equilibrium

To first validate the model's dynamics, simulations relative to the homeostatic equilibrium were run. The homeostatic equilibrium represents a state of the model where regardless of the absence of tumoral cells the overall dynamics still occur. This means that after the $1000\ MCS$ the system should still have the basal and luminal layers well defined and the four cell types that constitute the model should maintain their size and shape. This simulation was run for the standard values presented in Table 2 and Table 3 but without the replacement of a healthy cell by a tumoral cell. The result of one of the simulations is presented on Figure 8 where it is possible to visualize a top ($z = 150$) and a lateral ($x = 75$) view of the acinus.

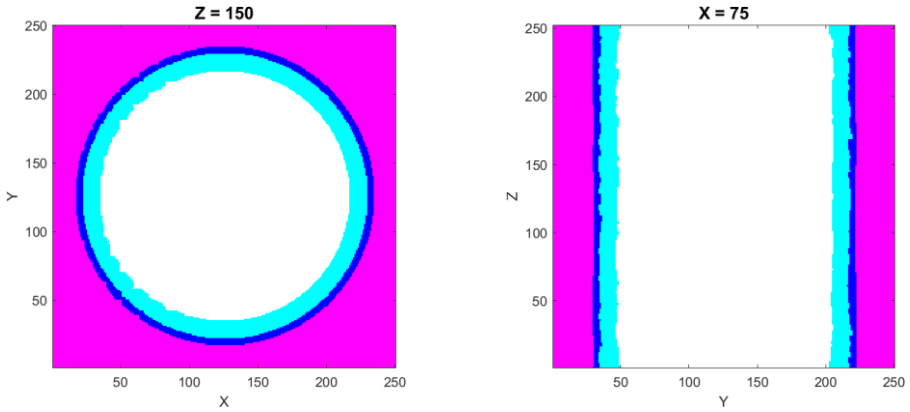

Figure 8 – Homeostatic Equilibrium – Acinus Top (left) and Lateral (right) Views

As it is possible to observe, although the basal and luminal cell layers have their limits less defined when compared to the initial state (Figure 4), the separation between the different cell types are maintained, as well as their dimensions and the overall system morphology. These results indicate that the chosen parameters are well adjusted for the normal model evolution and the systematic study can be based on them.

Normal Tumor Development

Once the homeostatic dynamics was tested and validated, every tumor-correlated parameter needs to be evaluated to ensure that the adenocarcinoma has a normal behavior. These evaluations involve checking model related aspects as well as those related to adenocarcinoma biology. The model aspects include determining whether the tumor has adequate space for growth or if it is limited by the model dimensions, verifying that the death pressure condition is being correctly applied, and ensure that the other cell parameters are accurate for the tumor cell parameters. The prostate tumor biological aspects are associated with the different steps of invasion of the prostate adenocarcinoma, as shown in Figure 5, specifically the lumen and healthy cells invasion should occur before reaching the stroma. Whenever a healthy cell parameter needs to be changed to adapt to a specific dynamic or condition, it is essential to repeat the process that validates the homeostatic equilibrium, as described in the previous section. Only after confirming that the change does not affect the way the homeostatic equilibrium occurs, the parameter adjustment can be made.

The values in Table 2 and Table 3 were obtained after these validation processes and every parameter and condition in the model is adjusted for a normal biological development. The simulation was run based on the standard conditions and the most relevant results obtained are shown in Figure 9, Figure 10, Figure 11, and Figure 12.

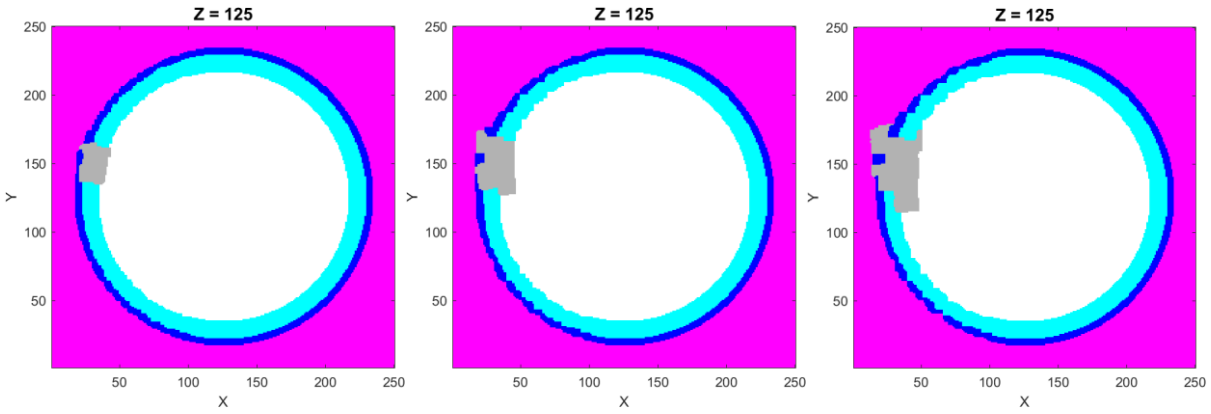

Figure 9 – Tumor Evolution as a function of MCS
Acinus Top View – 100 MCS (left), 350 MCS (middle), and 550 MCS (right)

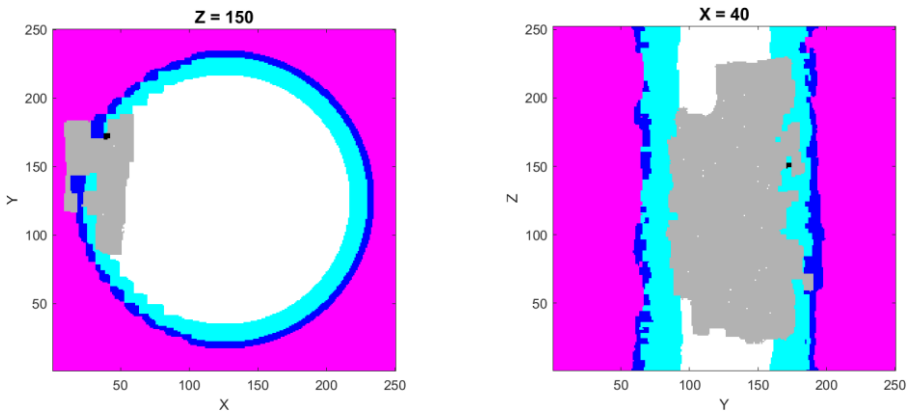

Figure 10 – Normal Tumor Growth (1000 MCS) – Acinus Top (left) and Lateral (right) Views

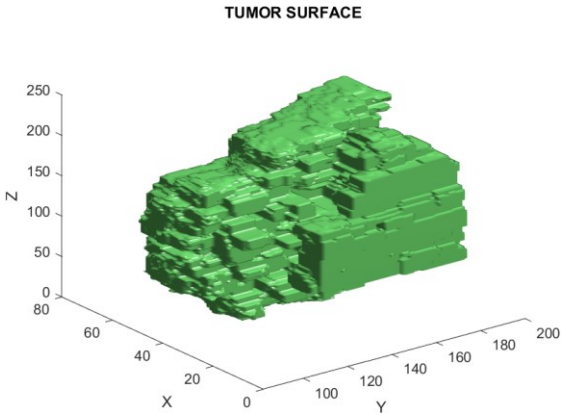

Figure 11 – Normal Tumor Growth – Tumor Morphology

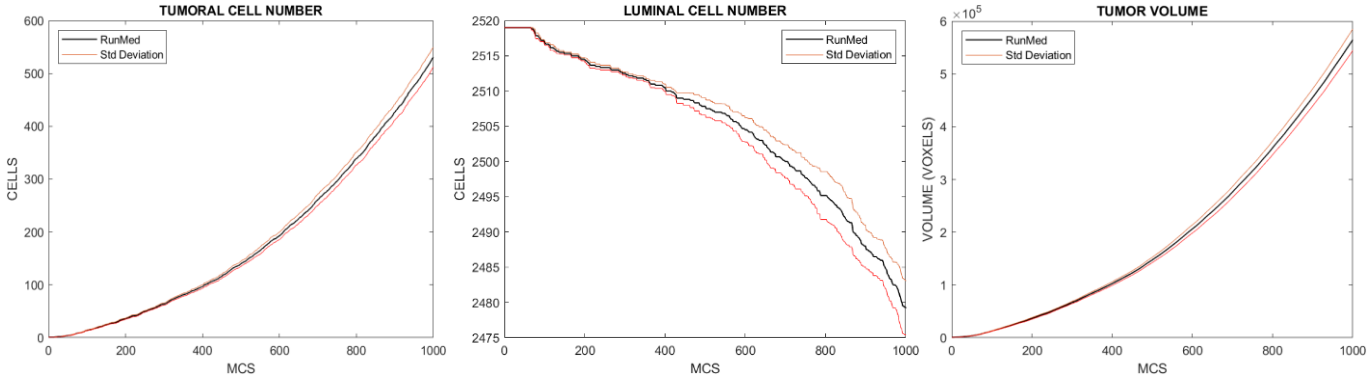

Figure 12 – Normal Tumor Growth
Number of Tumoral Cells (left), Luminal Cells (middle), and Tumor Volume (right) as a function of MCS
Bands Represent the Standard Deviation from the Mean Value of Six Runs

Based on the analysis of the three figures presented, it can be concluded that the obtained results are consistent with the expected outcomes. The evolution of the tumor development was measured as a function of time, and through the analysis of Figure 9 it is possible to conclude that the initial invasion was observed in the healthy cells (around $100\ MCS$) and lumen (around $350\ MCS$), followed by a stroma invasion stage (around $550\ MCS$), resulting in the final stage showed in Figure 10. The number of tumoral cells increased in an exponential way, along with the tumor volume (Figure 12), results that were also expected to occur. As the tumor grew, the luminal cells number decreased (Figure 12), as they were subjected to mechanical forces induced by the stiffness of the tumoral cells, which lead to their deaths. The number of basal cells was maintained constant throughout the simulation. Based on the different stages of the prostate adenocarcinoma presented in Figure 5 and the results obtained, it is possible to conclude that the tumor reached a stage between the latent and the clinical cases. The stromal invasion may be of great concern, since it facilitates the access of tumoral cells to blood vessels, thereby providing them with essential nutrients and oxygen to expand further. In a worst-case scenario, a stromal invasion may promote tumor proliferation to other regions of the body. This hypothesis, which will not be approached in this project, would need extra study to be confirmed.

Dependence of tumor development on the starting layer

The first systematic test performed was the dependence of the tumor development and growth with its initial layer. For this test, all the standard parameters were maintained except for the tumor starting layer which was switched to the basal cell layer. The position of the tumoral cell within the domain was consistent with that of the tumoral cell located on the luminal layer upon comparison. The most relevant results

obtained with the simulations are shown in Figure 13 and Figure 14. The tumor morphology is not presented in this case due to its high similarity to the morphology in the normal tumor growth (Figure 11).

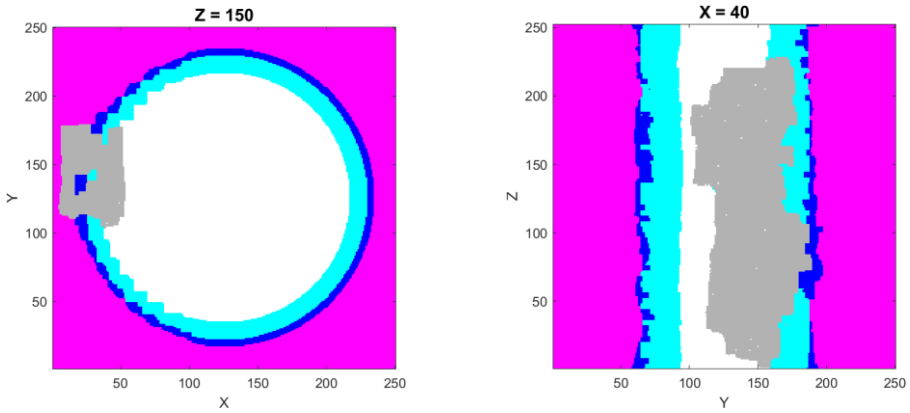

Figure 13 – Dependence on the Tumor Starting Layer (1000 MCS) – Acinus Top (left) and Lateral (right) Views

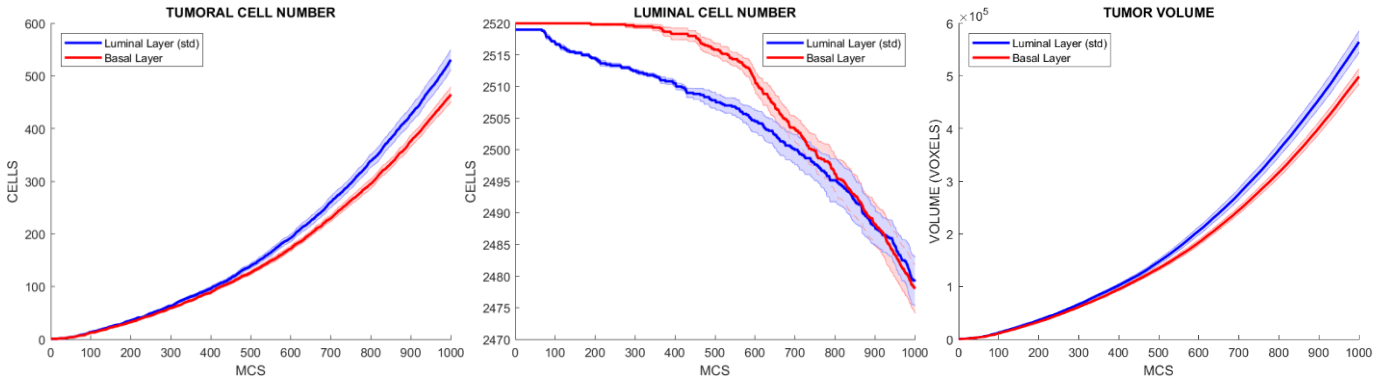

Figure 14 – Tumor Growth Dependence on the Tumor Starting Layer
Number of Tumoral Cells (left), Luminal Cells (middle), and Tumor Volume (right) as a function of MCS
Bands Represent the Standard Deviation from the Mean Value of Six Runs

Analyzing the Figure 13 and comparing it to the previous results of normal tumor development in Figure 10, it can be concluded that a tumor originating from a basal cell layer presents higher stroma invasion when compared to one with a luminal cell layer origin. Despite the slower adenocarcinoma development and the lower proliferation, the increased stromal invasiveness may facilitate the access of tumoral cells to blood vessels, as explained in the section above, resulting in the severe consequences described.

Upon analyzing the global results, it is possible to conclude that tumor development may exhibit a dependence on the tumor starting layer, despite the absence of a significant impact on its growth. This dependence has previously been investigated and studied in terms of prognostics and the progression of the adenocarcinoma itself, and the obtained results provide support for the dependence theory [11]. Additionally, it is possible to understand the results in terms of the dynamics of the system. As indicated by the results of the tumor development under the standard conditions, most of the tumor proliferation occurs in the lumen of the acinus, due to its lower stiffness. However, on an adenocarcinoma whose origin is a basal cell, the direct contact with the lumen is absent, and the tumor only interfaces with other basal cells, luminal cells, and the stroma. As these three cell types exhibit much higher inelasticity the tumor's ability to create space for growth is weakened, which results in a delayed growth until the lumen is reached.

Cell's Stiffness Influence on Tumor Development

In the developed model, cell's stiffness exerts a profound influence on the overall system dynamics. Changes in these parameters can give rise to substantial modifications on tumor progress, thereby underscoring its criticality. The inelasticity constants have a significant impact on the physical properties of the tissue cells, making them susceptible to deformations and dictating how each cell responds to mechanical stress. Stiffness also plays a crucial role in the cell's ability to create space for proliferation, particularly in tumoral cells, thus this parameter is expected to be of great influence on adenocarcinoma growth. Therefore, when the inelasticity constant of a cell, which is represented in the Hamiltonian parameter by $\lambda_V(\tau)$, is increased, the cell's resistance to mechanical pressures is enhanced, allowing it to reach its target volume faster when compared to a lower value of stiffness which will result on the opposite effect.

In this subsection, systematic studies were conducted by altering the stiffness of healthy and tumoral cells and analyzing the obtained results to verify their agreement with what was expected. The tumoral cells inelasticity constant was changed by a factor of 10% (Figure 15 and Figure 16), both in an upward and downward direction, while the same parameter was varied by a 50% factor on the basal and luminal cells (Figure 17 and Figure 18) and in the lumen (Figure 19). Apart from these changes, all the other parameters were maintained.

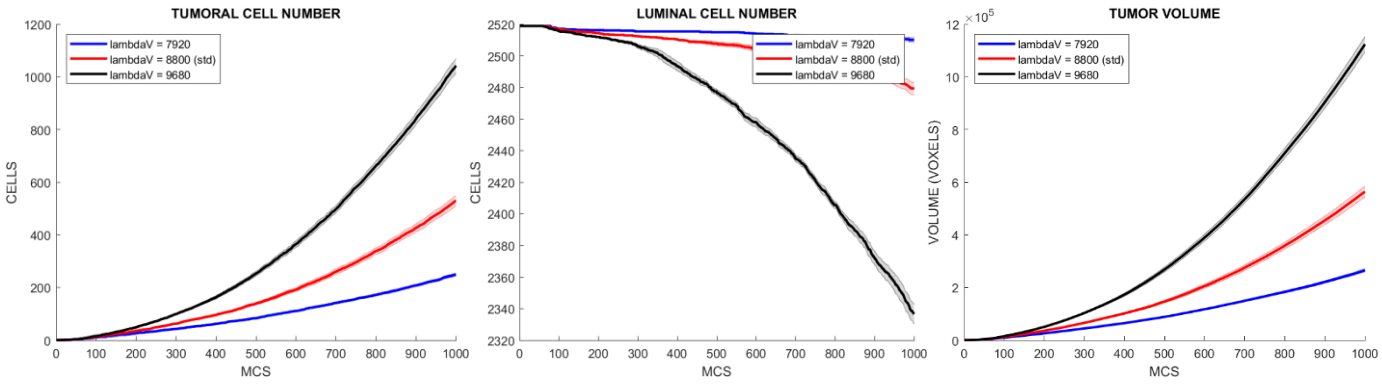

Figure 15 – Tumor Growth Dependence on the Tumoral Cell's Stiffness Parameter
Number of Tumoral Cells (left), Luminal Cells (middle), and Tumor Volume (right) as a function of MCS
Bands Represent the Standard Deviation from the Mean Value of Six Runs

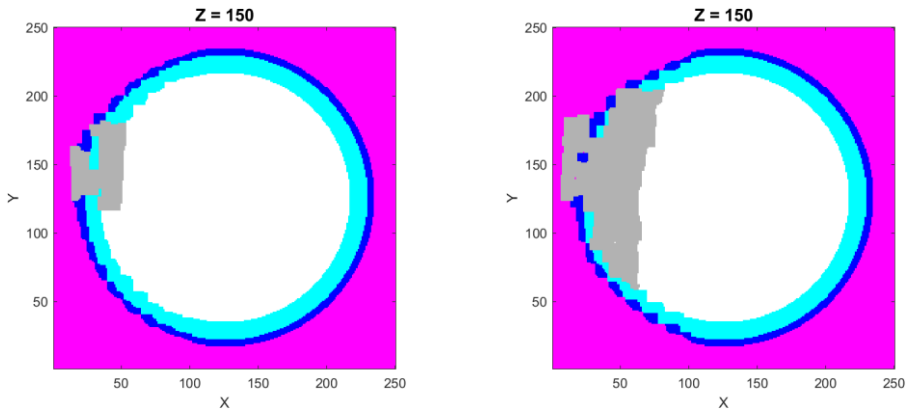

Figure 16 – Dependence on the Tumoral Cell's Stiffness Parameter (1000 MCS)
Acinus Top View – Stiffness Decrease (Left) and Stiffness Increase (Right)

Analyzing the Figure 15 it can be concluded that the stiffness of tumoral cells play, indeed, a crucial role in tumor development, as even a change of 10% in this parameter can have a significant impact of the final number of tumoral cells and the tumor volume. Particularly, the increase in the inelasticity constant results

in a tumor final volume that is more than twice the volume of the standard simulation, while the decrease in the same parameter led to a reduction of the tumor final volume by as much as half. Additionally, it is also important to understand that these changes also have an impact on tumor invasiveness. As it is possible to observe in Figure 16, a reduction in the stiffness of tumoral cells resulted in the development of a non-stromal invasive adenocarcinoma, as well as a less invasion on the lumen when compared to the results obtained in the standard tumor development (as shown in Figure 10). Upon comparison of these results with the various tumor stages presented in Figure 5, it can be inferred that only the prostatic intraepithelial neoplasia stage was reached at the end of the simulation. Furthermore, this decrease of the tumoral cell's inelasticity led to the survival of almost all luminal cells and all the basal cells. Upon examination of the Figure 16, it is evident that the 10% increase in the studied parameter resulted in a significantly higher invasion off all cell types, as compared not only to the decrease simulation, but also to the standard tumor development shown in Figure 10. The final stage of the adenocarcinoma can be considered an intermediate between the latent and the clinical stages, and the higher stromal invasion observed may result in contact with the blood vessels and, consequently, the access to nutrients and other parts of the body. Furthermore, in these simulations, the proliferation of tumoral cells through the luminal and basal layers was much more significant and led to the death of not only more luminal cells, but also of basal cells.

Additional tests regarding the tumoral cells stiffness were conducted by varying this parameter by a 50% factor. As expected, the differences in tumor volume and tumoral cell number were very significant. For the parameter decrease simulations, the final volume was reduced by a one hundred factor and only about five tumoral cells existed at the last MCS. When the parameter suffered a 50% increase, the tumoral cells growth rate was so high that they were limited by the system dimensions around the 600 MCS. As these were the expected results, no more tests were done regarding this parameter.

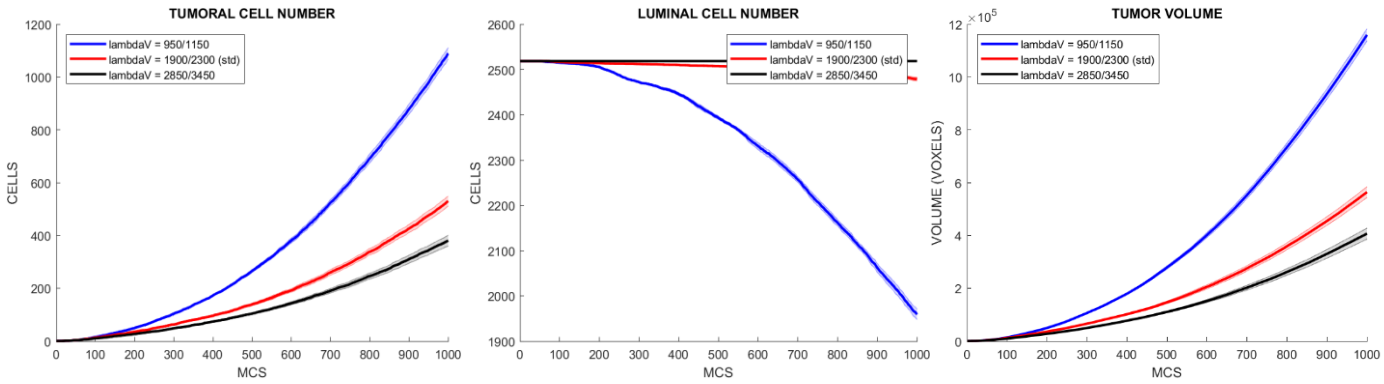

Figure 17 – Tumor Growth Dependence on the Luminal and Basal Cell's Stiffness Parameter
Number of Tumoral Cells (left), Luminal Cells (middle), and Tumor Volume (right) as a function of MCS
Bands Represent the Standard Deviation from the Mean Value of Six Runs
First and Second Values in the Legend correspond to the Luminal and Basal Cells Stiffness, respectively

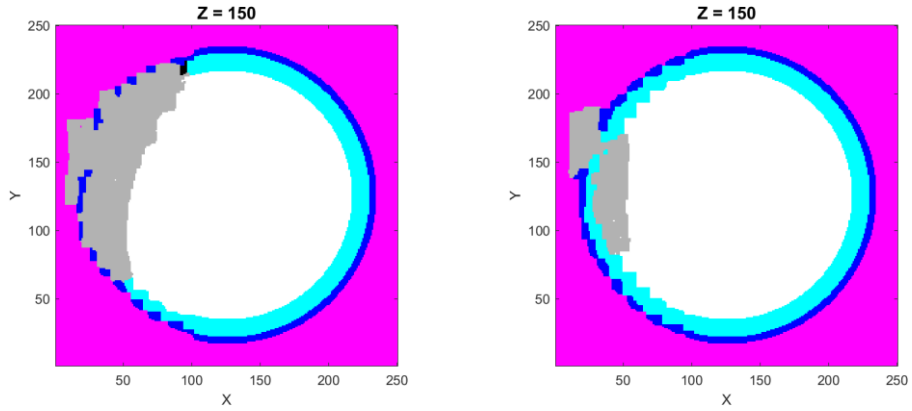

Figure 18 – Tumor Growth Dependence on Luminal and Basal Cell's Stiffness Parameter (1000 MCS) Acinus Top View – Stiffness Decrease (Left) and Stiffness Increase (Right)

Upon analyzing Figure 17, which depicts the variation of the luminal and basal cells' stiffness by a 50% factor, it is evident that significant changes in tumor development occurred. The inelasticity constant values are represented first for the luminal cells and then, after the slash, the corresponding value for the basal cells. When the parameters were decreased, the tumor had a more significant development when compared to the growth with the standard parameters. Upon comparison of the final tumor volume and the number of tumoral cells with the standard value and the decreased healthy cells' stiffness, it is possible to observe a doubling in both values. Through the observation of Figure 18 and its comparison to Figure 5, it can be concluded that the evolution stage of the adenocarcinoma reached at the end of the simulation was an intermediate stage in between the latent and clinical phases. The attainment of this stage once more implies that the tumoral cells may have direct access to blood vessels leading to the consequences previously explained. Lastly, it is important to mention the influence that these changes had on the number of healthy cells in the model. The decrease of their stiffness meant a lower resistance to the mechanical stress imposed by the tumoral cells, which, as anticipated, led to increased mortality rates, not only in luminal cells but also in basal cells. Examining the increase of the inelasticity constant of the healthy cells, a reduction in both the number of tumoral cells and the tumor volume is seen. Despite this occurrence, the impact caused was not as significant as the effects that arose from the decrease in the parameters. Additionally, in Figure 18, it is possible to view an adenocarcinoma with lumen and stromal invasiveness, therefore, as described in Figure 5, the tumor reached the latent cancer stage and did not pass through the clinical stage. Once again, these types of adenocarcinomas may have easier access to nutrients and oxygen, as well as other parts of the body, by directly contacting blood vessels. The other positive aspect, apart from the slower tumor development, is the fact that neither the luminal nor the basal cells have died in any of the simulations, resulting on the preservation of the acinus integrity.

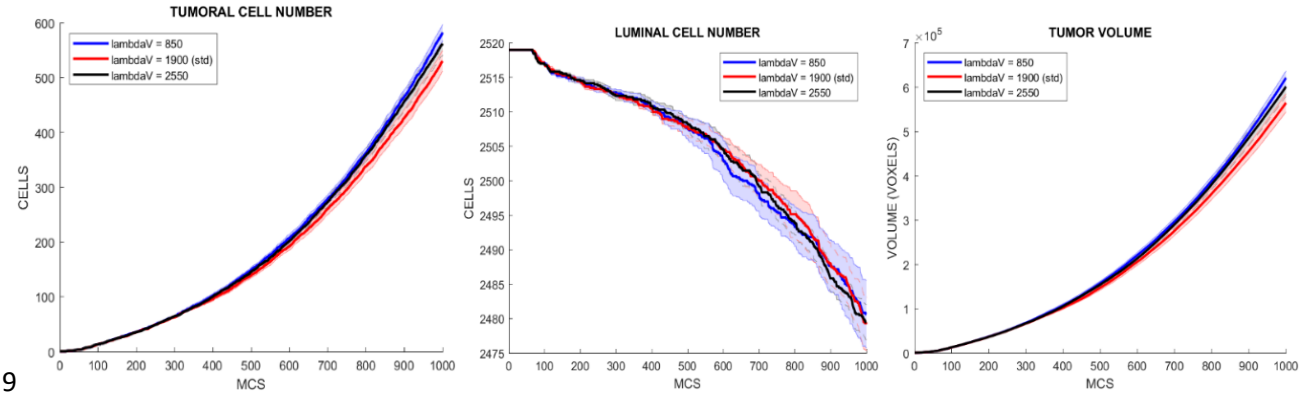

9

Figure 19 – Tumor Growth Dependence on the Lumen Stiffness Parameter
Number of Tumoral Cells (left), Luminal Cells (middle), and Tumor Volume (right) as a function of MCS
Bands Represent the Standard Deviation from the Mean Value of Six Runs

Regarding the simulations relative to the manipulation of the lumen stiffness parameter, from the obtained results, depicted in Figure 19, are sufficient to understand the changes induced in the model. As it is possible to visualize, neither the decreasing nor the increasing of the parameter had a significant effect on the model's characteristics, a predictable outcome. The number of tumoral cells was approximately maintained, and the same was verified for the tumor volume and for number of luminal and basal cells. This phenomenon can be explained by the fact that the lumen was modeled as one single cell with a large volume, and its inelasticity is lower (when compared with the relative volume) than the other cell types since it represents a liquid, which is more flexible and malleable than cells with defined borders. Hence, when the lumen loses voxels, the weight of this loss in the global Hamiltonian is pretty much imperceptible when compared to one produced by the voxels gain of a tumoral cell, for example. It was thus expected that a change of the lumen's inelasticity by a 50% factor would not produce significant alterations in the overall model.

To complete the study of this parameter, a set of new simulations were run, where the inelasticity was increased to twenty times its standard value, to check if the tumor development was retarded in any way. As no change was observed from the previous results, the graphs obtained are not shown. Even with this increase, the changes produced in the adenocarcinoma were negligible, as the tumor related parameters remained approximately constant, since the loss of voxels by the lumen continued to represent an insignificant part of the energy on the global Hamiltonian upon comparison to the energy impact of the voxels gain of tumoral cells.

Reviewing all the obtained results regarding the change of cells stiffness and the conclusions taken from them, an overall view of each cell, as well as its influence can be presented, and possible therapeutic targets can be suggested. Regarding the tumoral cells, it was seen that their inelasticity constant was of great influence in the tumor development. Hence, through the targeting of the pathways that regulate the mechanical properties of the tumoral cells it is highly probable that the adenocarcinoma growth rate will be decreased, and the clinical invasive state may not be reached, maintaining the prostate integrity. The basal and luminal cells stiffness was also found to be of great importance, as their increase led to a less aggressive adenocarcinoma and the prostate integrity was preserved, meaning that the change in the healthy cells mechanical resistance could also be a goal to consider. However, it is important to bear in mind that this change could have other possible side effects as it does not target the tumoral cells specifically, but instead healthy cells whose mechanical characteristics are adjusted for a homeostatic equilibrium. Besides this, the stroma invasion was not avoided and possibly the access to blood vessels by the tumoral cells may lead to other dangerous consequences. Analyzing the lumen inelasticity changes, the results demonstrated that due

to the fact that it is a liquid, hence the stiffness is much lower, even the increasing of the value by non-possible biological factors made hardly any difference in the overall tumor development.

Adhesion Energy and Tumor Development

Adhesion energy is the parameter which regulates the surface interaction between two different cells and its value is predicted to be of great influence, potentially surpassing the importance of the cells' stiffness parameter. It is correlated with the cellular adhesion through an inverse proportionality constant, which means that a higher adhesion energy leads to a lower adhesion between two cells, and a lower adhesion energy creates the opposite effect, a higher adhesion between two cells. In the Hamiltonian energy, the adhesion energy is represented by the $J_{\tau\tau'}$ parameter.

In this subsection, the systematic studies conducted on the adhesion energy parameter considered two distinct scenarios. In the first one, the adhesion energy was modified for every cell within the system, including healthy cells. This involved varying this parameter both downwards and upwards from its standard value ($J_{\tau\tau'} = 2.55$ presented in Table 2). Hence the new values considered for the adhesion energy were $J_{\tau\tau'} = 2.3$, $J_{\tau\tau'} = 2.8$ and $J_{\tau\tau'} = 3.06$. The most relevant results from these simulations are presented on Figure 20 and Figure 21. The second scenario was created through the manipulation of the adhesion energy only of tumoral cells. This meant that all healthy cells (lumen, luminal cells, basal cells, and stroma) had their adhesion energy parameter unchanged from the standard value (presented in Table 2), while the tumoral cells' adhesion energy parameter was changed from its standard value to the values used in the first scenario, $J_{\tau\tau'} = 2.3, J_{\tau\tau'} = 2.8$ and $J_{\tau\tau'} = 3.06$. The results that primarily enabled to retrieve conclusions from the tests are shown in Figure 22. It is important to remember that the values presented are relative to the adhesion energy of cells of different types. The adhesion energy between two cells of the same type is obtained by multiplying the value by a 0.9 factor (the same was done to obtain the values of the adhesion energy in Table 2). Apart from the mentioned changes, every other parameter in the model remained unchanged.

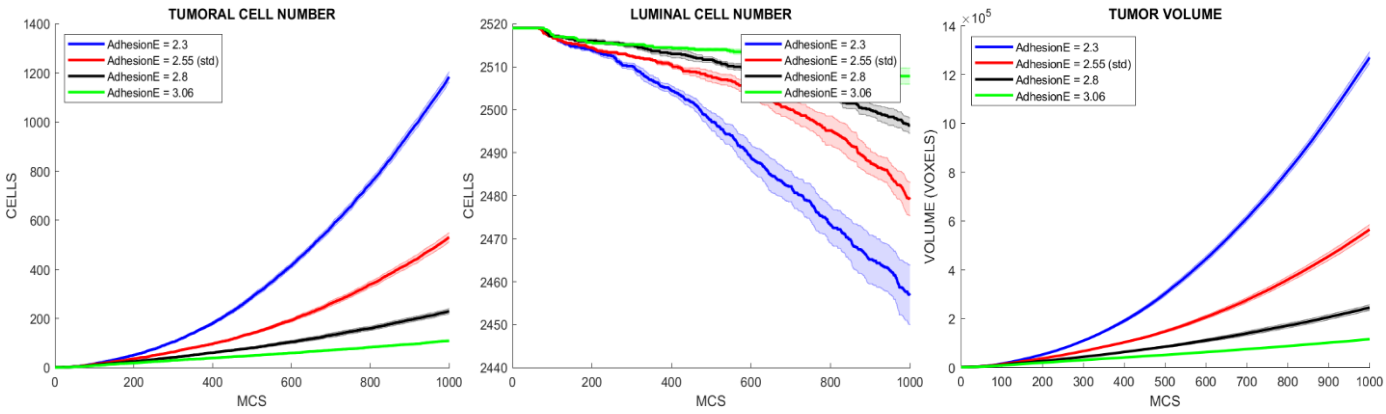

Figure 20 – Tumor Growth Dependence on Adhesion Energy of All Cells
Number of Tumoral Cells (left), Luminal Cells (middle), and Tumor Volume (right) as a function of MCS
Bands Represent the Standard Deviation from the Mean Value of Six Runs

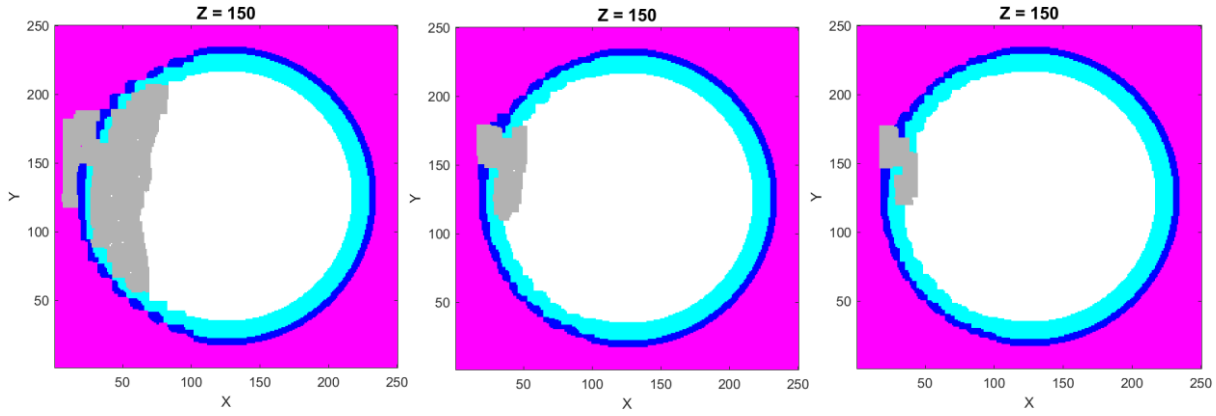

Figure 21 – Tumor Growth Dependence on the Adhesion Energy Parameter (1000 MCS) Acinus Top View – $J_{\tau\tau'} = 2.3$ (Left), $J_{\tau\tau'} = 2.8$ (Middle) and $J_{\tau\tau'} = 3.06$ (Right)

Upon analyzing Figure 20, which illustrates the influence of decreasing or increasing the adhesion energy for every cell in the considered model, it is possible to conclude that the expected results were not reached. It was anticipated that a higher adhesion energy parameter would lead to less cohesive cells, meaning that the tumor could create more space to expand itself with less effort. However, contrary to expectations, the exact opposite of what was predicted happened. A higher adhesion energy (smaller cell adhesion) led to a less aggressive adenocarcinoma, which exhibited a slower growth when compared to the other values for this parameter. For the minimal value of the adhesion energy parameter used, the tumor final volume was diminished by a factor of 6, as well as the tumoral cells number. Conversely, as the adhesion energy was decreased, hence an increased cellular adhesion, the tumor growth was more noteworthy, leading to a final tumor volume that reached more than 200% the volume observed in the simulations under the standard conditions. The unforeseen results can be explained by a mechanical phenomenon called cell collective migration, which is a common phenomenon during adenocarcinoma metastasis [23]. Upon increasing the adhesion between cells due to a decrease of the adhesion energy, all system cells (tumoral and healthy) are compelled to move in a collective way. Cell collective movement induces an increased pressure in the vicinity of healthy cells which yields to tumoral cells, who have a higher stiffness. So, even if the tumoral cells specific mobility is reduced, the microenvironment around the tumor moves collectively creating a high-pressure environment that is beneficial to tumoral cells as they are more tolerant to such conditions. Consequently, this leads to a more aggressive tumor behavior and consequently a higher rate of tumor growth.

Apart from the tumor growth it is also important to analyze the final stage of the tumor for each scenario. Decreasing the adhesion energy ($J_{\tau\tau'} = 2.3$) led to a final adenocarcinoma that can be positioned between the latent and clinical stages of tumor development, as it was observed upon comparison of the result (left imaged of Figure 21) with Figure 5. On the other hand, increasing the adhesion energy to values of $J_{\tau\tau'} = 2.8$ and $J_{\tau\tau'} = 3.06$ led to the outcomes shown in the middle and right portions of Figure 21. As it is possible to observe, the acinus structure was maintained in both situations and the resulting tumor never reached the full stromal invasiveness, meaning that the adenocarcinoma clinical state was not reached. This could be beneficial to the patient as the stromal invasion could lead to direct access to blood vessels, as explained in the previous subsections. Comparing both cases shown in the figure with the stages present in Figure 5, it is possible to conclude that for the value of $J_{\tau\tau'} = 2.8$, the tumor could be considered in an early stage of a prostatic intraepithelial neoplasia, while for the value of $J_{\tau\tau'} = 3.06$ the prostatic intraepithelial neoplasia stage was arguably reached as there was almost no lumen invasion.

To finalize the study of the adhesion energy parameter for all system cells, a posterior set of simulations were run where not only the adhesion energy parameter was decreased but also the tumoral cells stiffness was reduced by a factor of 0.9. This test was performed to verify if the initial theory that a higher adhesion between cells would mean that the cohesiveness of the healthy cells would create a stricter environment

reducing the tumoral cells proliferation. However, even in this case, the collective invasion factor prevailed, and the obtained results were similar to the previous ones (results not shown).

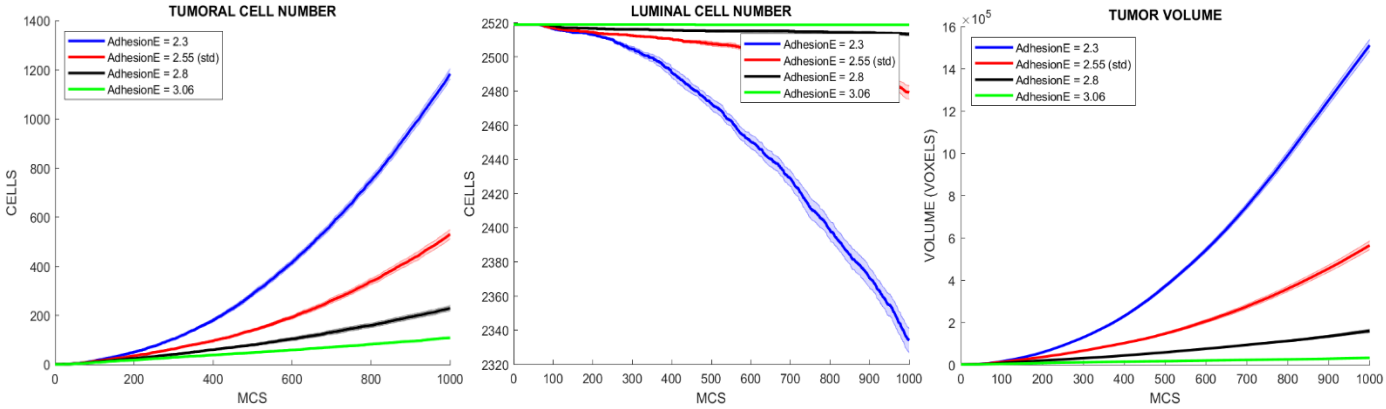

Figure 22 – Tumor Growth Dependence on Adhesion Energy of Tumoral Cells
Number of Tumoral Cells (left), Luminal Cells (middle), and Tumor Volume (right) as a function of MCS
Bands Represent the Standard Deviation from the Mean Value of Six Runs

Regarding the modifications made solely to the adhesion energy of tumoral cells, it is possible to observe in Figure 22 a high similarity upon comparison to the previous results presented in Figure 20, where the adhesion energy parameter was altered for each cell of the model. Once more, even though a lower adhesion energy, meaning a higher adhesion between cells, could potentially pose a challenge to the tumor capability of creating space for its growth, the collective migration of the tumor and its surrounding cells remained more significant. In the cases where the parameter was increased the tumor volume and number of cells diminished and the opposite happened when the adhesion energy was increased. However, it is important to notice that the final characteristics of the model, specifically the number of tumoral cells and the tumor volume were more significantly influenced by the alteration of solely the tumoral cells adhesion energy. For instance, in the case of $J_{\tau\tau'} = 3.06$, the results shown in Figure 22 demonstrate that a lower tumor volume and tumoral cell number is obtained at the end of the simulation when compared to the results obtained in Figure 20 for the same value. On the opposite, the results in Figure 22 show that decreasing of adhesion energy to $J_{\tau\tau'} = 2.3$ led to a tumor volume that is slightly higher and has an increased number of tumoral cells compared to the results for the same value presented in Figure 20. The adenocarcinoma stages reached in the simulations of Figure 22 were approximately equal to the corresponding phases observed in the previous simulations shown in Figure 20, considering the variations in the adhesion energy values.

In conclusion, based on the obtained results, it can be said that the adhesion energy has indeed a great impact on tumor development, as it can promote a cellular migration behavior in the cells that changes the rate at which tumor proliferation occurs. Therefore, a clue for a possible therapeutic target is modifying the biological mechanisms that control the adhesion between the cells where the adenocarcinoma was formed. Targeting the tumoral cells adhesion, making them less cohesive to the stroma, lumen, and other cells in the prostate tissue, will allow to control in a more effective way the tumor development when comparing to a decrease in all cell's adhesion. Despite this, the decreasing of the adhesion of all the biological elements of the glandular structure would also be of great influence in the overall tumor growth, however, in this case, it needs to be considered that changing a standard biophysical parameter of healthy cells could lead to an unexpected behavior of the whole system.

Tumoral Cells Proliferation Cycle

The last systematical study on the model parameters focused on extending the duration of the tumoral cell cycle [24]. As it was previously explained, tumoral cells require a certain lifetime before proliferation and

mitosis occurs, as the presence of certain organelles and structures are essential for the subsequent proliferation of the two new cells. An effective and straightforward approach to controlling tumor growth is to increase the proliferation time limit, which leads to a lower proliferation rate due to the increased cell cycle duration. In this subsection, the standard value for this parameter shown in Table 2 was increased from $25\ MCS$ to $36\ MCS$ and $48\ MCS$. The results which represent the temporal evolution of the most crucial parameters as well as the top view of the acinus, for the increased time proliferation limit, is presented in Figure 23 and Figure 24, respectively.

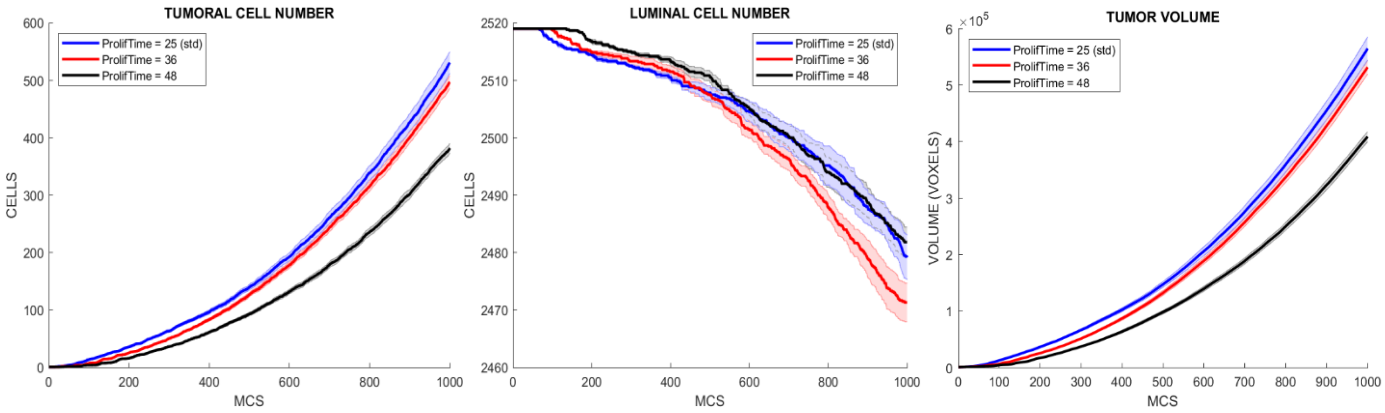

Figure 23 – Tumor Growth Dependence on the Proliferation Time Limit
Number of Tumoral Cells (left), Luminal Cells (middle), and Tumor Volume (right) as a function of MCS
Bands Represent the Standard Deviation from the Mean Value of Six Runs

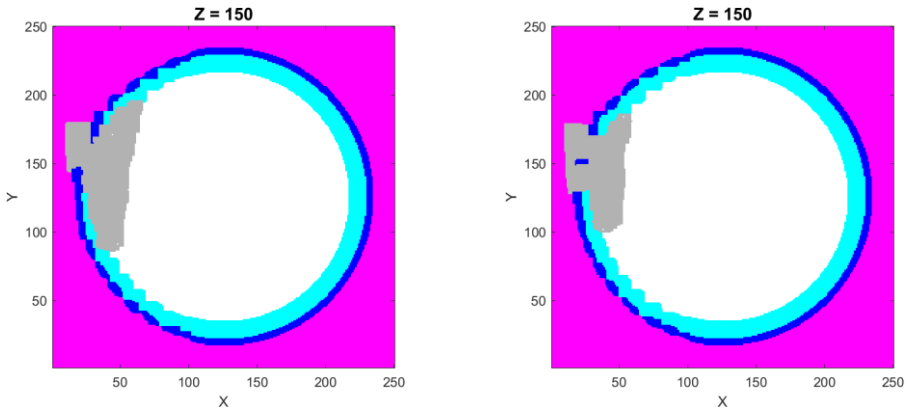

Figure 24 - Tumor Growth Dependence on the Proliferation Time Limit (1000 MCS)
Acinus Top View – Proliferation Time 36 (Left) and Proliferation Time 48 (Right)

Through the analysis of Figure 23, the empirical evidence supports the hypothesis that extending the cell proliferation time limit would lead to a less aggressive tumor, with a more controlled proliferation. The increasing of the proliferation time limit to $36\ MCS$ led to a decrease in the tumor volume and in the number of tumoral cells, however, it was not significant. However, a change in the studied parameter from the standard value to $48\ MCS$ resulted in a substantial decrease in the tumor final volume and number of tumoral cells as it only reached around two-thirds of the value obtained under the standard conditions. Additionally, another set of simulations were conducted where the proliferation time limit was increased to a value of $60\ MCS$ to verify if the pattern was maintained. In this case, the tumor growth was significantly slowed as the tumor specific characteristics, specifically the tumor volume and the number of tumoral cells, decreased to less than a third of the values obtained in the standard conditions, as expected. Even though the increasing of the proliferation time limit led to a slower growth rate of the adenocarcinoma, the number of healthy cells that died throughout the simulation was approximately the same for the increased values and the standard conditions as viewed in Figure 23.

Regarding the tumoral stages attained in each value of the proliferation time limit, both the increase to $36\ MCS$ and to $48\ MCS$ led to an intermediate phase between the latent and clinical stages as both lumen and stromal invasion occurred. Once again, it is crucial to acknowledge that stromal invasion can lead to further complications as direct access to blood vessels is an option to consider. This phenomenon carries significant consequences that can contribute to uncontrolled tumor growth, as explained before.

From the results above, it is possible to conclude, in accordance to the expected, that the increasing duration of the tumoral cells proliferation cycle impacted the tumor growth in a positive way, as the adenocarcinoma was less aggressive and progressed more slowly. Therefore, modifying the proliferation rate through the increasing of the proliferation time limit is a good strategy to control the tumor and so a possible therapeutic target.

Conversion of Voxel Size and MCS to Real Units

To conclude the results section, it is necessary to convert the model units to real measurement units. This conversion is essential for translating the achieved results into applicable real-world values. Firstly, the conversion from the voxel edge segment to micrometers (μm) will be presented and secondly, the conversion from the model time unit, the Monte Carlo Step (MCS), to real time, specifically months, will be discussed.

To convert the voxel edge segment to micrometers, a simple correlation between one of the cells' real size in micrometers and the size in voxels of that same cell in the model must be set, recurring to the literature and to histological images (the values in Table 1). Taking the case of the luminal cells to proceed with the conversion, their depth is approximately $20\mu m$. By analyzing the luminal cells in the model, it is possible to conclude that their average depth is composed of around 13 voxels. Being the voxels cubic, which means that all lateral segments have the same length, the relation between the model and the reality can be established by the following equation:

$$Voxel_{edge\ segment} = \frac{1 \times 20}{13} \approx 1.54\ (\mu m)$$

The same conversion could be done using other dimensions of the luminal cells (height or width) or even using other cell types. Using the final tumor volume obtained in Figure 12, it is possible to calculate how many cubic centimeters (cc) it would correspond in real units through the calculus of each voxel volume and then multiplying by the number of voxels, as follows:

$$V_{voxel} \approx 1.54^3 \approx 3.65(\mu m^3) = 3.65 \times 10^{-9}(cc)$$

Comparing the obtained value for the final tumor volume with values shown in literature [25], the modeled adenocarcinoma's volume is much smaller. However, this result was predictable as in the considered model only one acinus was represented, and the prostate gland is divided into several tubuloalveolar glands and each one of these contains multiple acini.

Regarding the conversion from the model time unit to real time units, it is crucial to determine the doubling time [25] of the prostate adenocarcinoma. The doubling time represents the time required for the tumor to double in volume under certain conditions. Therefore, the doubling time needs to be considered in a real prostate environment as cells in culture have an easier access to nutrients and spatial constraints are not present, which can significantly increase their growth rate. Upon analyzing the studies conducted on prostate adenocarcinoma, it can be concluded that the prostate adenocarcinoma doubling time varies accordingly to the stage of the tumor and the corresponding Gleason grade [26]. The range of values for the tumor volume doubling time is from one to six years [27]. Analyzing the results depicted in Figure 12, which illustrate the outcomes under the standard simulation conditions, it was observed that the adenocarcinoma required approximately $200\ MCS$ to expand in size from 200,000 to 400,000 voxels of volume. Considering a

median doubling time of around three years, and the time the modeled tumor needed to double in volume, the following expression, which relates both results and represents the duration of each MCS, can be written:

$$MCS = \frac{3\ years}{200\ MCS} = 0.015(years) \approx 5.5(days)$$

Discussion

The current work presents a computational model of the prostatic adenocarcinoma initiation and its progression until a clinical state is reached. Stochastic simulations under diverse conditions and parameters values were run to check for possible therapeutic targets regarding prostate cancer. The results obtained from these studies allowed to confirm that a realistic simulation of the cancer initiation on the prostate gland was developed and reasonable clues into how to control its' growth were produced.

It was possible to conclude that depending on the tumor starting layer, luminal or basal cell layer, different outcomes can arise. Even though a tumor with basal cell layer origin has a lower growth rate and both cases led to a final adenocarcinoma classified between latent and clinical stages, the stromal invasion on basal cell layer simulations was more significant. Stromal invasion implies that the basal membrane was ruptured and direct access to the stromal blood vessels needs to be held in account. The danger of this invasion arises from the fact that nutrients and oxygen that flow through the blood vessels can be easier to access by the tumoral cells. Additionally, the ability of the cancer cells to metastasize other body regions could lead to further complications.

Regarding the mechanical parameters in the model that influence the facility with which the adenocarcinoma can create space to grow and possibly kill healthy cells, the results showed promissory therapeutic targets. The tumoral cells stiffness parameter is highly sensible, as even slight changes from the standard value can lead to very distinct results. An increase in the parameter value leads to a high-pressure placed in healthy cells which cannot mechanically resist and end up dying. This result in the loss of the acinus structure and a high stromal invasion. On the other hand, a decrease in this parameter led to a less invasive tumor, with high difficulty in creating space to grow, resulting in the survival of almost every cell in the system and the preservation of the acinus three-dimensional geometry. Changes in the stiffness of luminal and basal cells also have an impact on tumor development, even though not as relevant. An increase of this parameter resulted in the maintenance of the acinus structure, however, luminal and stromal invasion are still present which can lead to potential risks. The changes in lumen stiffness were not significant as the tumor development was hardly decreased by the increase of the respective parameter, as the results demonstrated.

Adhesion energy is one of the most relevant characteristics of the model, which affects in a significant way tumor growth. It is related to collective invasion, a phenomenon where the higher adhesion between cells, obtained through the decrease of the adhesion energy, leads to a unified movement which creates space for tumor proliferation. This process forces all cells around the tumor to move in a collective way, which compensates for the tumoral cell reduced motility. The opposite effect was observed when the adhesion energy was increased, and consequent decrease of cell to cell adhesion. The tumor was less aggressive, and the growth rate diminished due to decreased collective migration. These tests were done by manipulating the adhesion energy for each cell in the model or solely for tumoral cells. The results showed that both led to evident changes in the tumor growth rates. However, the manipulation of the parameter only for tumoral cells had a more significant impact.

Lastly, one of the most evident and effective manners of controlling tumor proliferation is through the manipulation of the tumoral cell cycle duration. By increasing the proliferation time limit of tumoral cells, their proliferation rate will automatically be diminished. This will result in a less aggressive tumor which can be more controllable.

From this study, it can be suggested that target specific mechanical cell characteristics such as the tumoral, luminal, and basal cells' inelasticity's constants, the adhesion energy of all cells or solely of tumoral cells and tumoral cell cycle duration can be measures applied to prevent a faster tumor development and its advance into more threatening stages, such as metastasis.

Future Work

Based on the available scientific literature and the obtained results, the current model can be enhanced to achieve a more accurate simulation of the tumor dynamics within a real prostate environment. Future research on this topic could focus on incorporating a more complex prostate geometry, particularly by representing multiple acini or, if possible, a complete tubuloalveolar gland, to create a more realistic model. By adopting this comprehensive geometry, different tumor developments could be studied and a comparison between the results and the Gleason criteria could be established. A new geometry that models two interconnected acini has already been developed, as observed in Figure 25. Additionally, incorporating blood vessels in the stroma and studying the influence produced by this alteration in the tumor development is also an improvement to be considered. A new term can be incorporated in the Hamiltonian, to represent the contact between tumoral cells and blood vessels, as access to essential nutrients and oxygen is facilitated. By including blood vessels, a more comprehensive understanding of tumor progression can be achieved. Moreover, it would be beneficial to model existing therapies to gain insight into the occurrence and mechanisms behind tumor regrowth associated with each treatment option. This could provide cues to how different therapies affect tumor dynamics and possibly aid the development of new and more effective strategies.

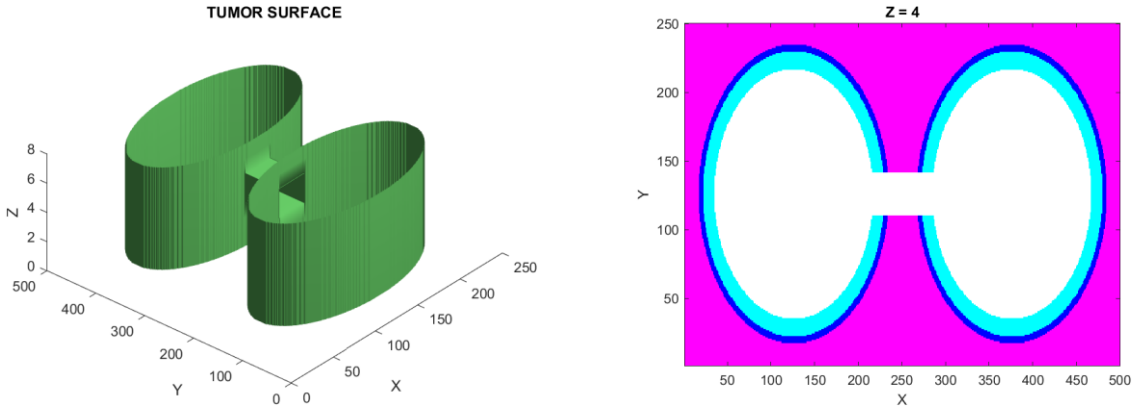

Figure 25 – New Geometry Morphology (left) and New Geometry Top View (right)

Conclusions

Throughout the semester, under the guidance of professors João Carvalho and Rui Travasso, a simplified three-dimensional computational model of tumor initiation and development in a small domain of the prostate was designed, developed, and tested. The model describes the domain of one acinus by representing the cellular layers observed on histological images and the initiation and progress of an adenocarcinoma. The studies conducted were evaluated using metrics related to the main characteristics of the tumor development, specifically its volume, number of tumoral cells, death of healthy cells and invasion of the surrounding tissues (mainly the stroma). These measurements allowed to describe the adenocarcinoma development (including the comparison to clinical stages) and gain insights on how the system parameters affect tumor growth. Computational modeling was an essential tool to this project, as *in silico* environments allow a quick and inexpensive study of different biological scenarios as well as individual study of complex phenomena. New insights on possible therapeutic targets can also arise from the *in silico* testing of different hypotheses, without posing possible ethical problems. Even though the model still has some room for improvement, the mechanical characteristics studied provided a plausible understanding of tumor development and potential therapeutic targets. Their effect in better controlling adenocarcinoma growth and invasiveness was notable, suggested by the obtained results.

References

[1] Carvalho J., Lopes V., Travasso R., A three dimensional computer model of urothelium and bladder cancer initiation, progress and collective invasion, Informatics in Medicine Unlocked, Volume 26, 2021, 100750, ISSN 2352-9148, https://doi.org/10.1016/j.imu.2021.100750

[2] J. Carneiro e L. C. Junqueira, Histologia Básica Texto & Atlas, 13 ed., G. Koogan, Ed., 2017, p. 568.

[3] Lee, C. H., Akin-Olugbade, O., & Kirschenbaum, A. (2011). Overview of prostate anatomy, histology, and pathology. *Endocrinology and metabolism clinics of North America*, *40*(3), 565–ix. https://doi.org/10.1016/j.ecl.2011.05.012.

[4] F. H. Netter, Atlas of Human Anatomy, 6 ed., Saunders/Elsevier, 2008, p. 640.

[5] Ittmann M. (2018). Anatomy and Histology of the Human and Murine Prostate. *Cold Spring Harbor perspectives in medicine*, *8*(5), a030346. https://doi.org/10.1101/cshperspect.a030346.

[6] [Online]. Available: http://histologyguide.com/. [Accessed 26 4 2023].

[7] Salem, O., & Hansen, C. G. (2019). The Hippo Pathway in Prostate Cancer. *Cells*, *8*(4), 370. https://doi.org/10.3390/cells8040370.

[8] [Online]. Available: https://prostatecanceruk.org/prostate-information-and-support. [Accessed 27 4 2023].

[9] Sekhoacha, M., Riet, K., Motloung, P., Gumenku, L., Adegoke, A., & Mashele, S. (2022). Prostate Cancer Review: Genetics, Diagnosis, Treatment Options, and Alternative Approaches. *Molecules (Basel, Switzerland)*, *27*(17), 5730. https://doi.org/10.3390/molecules27175730

[10] [Online]. Available: https://www.cancer.org/cancer/prostate-cancer.html. [Accessed 27 4 2023].

[11] Wang, G., Zhao, D., Spring, D. J., & DePinho, R. A. (2018). Genetics and biology of prostate cancer. *Genes & development*, *32*(17-18), 1105–1140. https://doi.org/10.1101/gad.315739.118

[12] Epstein, J. I., Zelefsky, M. J., Sjoberg, D. D., Nelson, J. B., Egevad, L., Magi-Galluzzi, C., Vickers, A. J., Parwani, A. V., Reuter, V. E., Fine, S. W., Eastham, J. A., Wiklund, P., Han, M., Reddy, C. A., Ciezki, J. P., Nyberg, T., & Klein, E. A. (2016). A Contemporary Prostate Cancer Grading System: A Validated Alternative to the Gleason Score. *European urology*, *69*(3), 428–435. https://doi.org/10.1016/j.eururo.2015.06.046

[13] Barakzai M. A. (2019). Prostatic Adenocarcinoma: A Grading from Gleason to the New Grade-Group System: A Historical and Critical Review. *Asian Pacific journal of cancer prevention : APJCP*, *20*(3), 661–666. https://doi.org/10.31557/APJCP.2019.20.3.661

[14] Epstein J. I. (2018). Prostate cancer grading: a decade after the 2005 modified system. *Modern pathology : an official journal of the United States and Canadian Academy of Pathology, Inc*, *31*(S1), S47–S63. https://doi.org/10.1038/modpathol.2017.133

[15] van Leenders, G. J. L. H., Verhoef, E. I., & Hollemans, E. (2020). Prostate cancer growth patterns beyond the Gleason score: entering a new era of comprehensive tumour grading. *Histopathology*, *77*(6), 850–861. https://doi.org/10.1111/his.14214

[16] Evans A. J. (2018). Treatment effects in prostate cancer. *Modern pathology : an official journal of the United States and Canadian Academy of Pathology, Inc*, *31*(S1), S110–S121. https://doi.org/10.1038/modpathol.2017.158

[17] Ji, Z., Yan, K., Li, W., Hu, H., & Zhu, X. (2017). Mathematical and Computational Modeling in Complex Biological Systems. *BioMed research international*, *2017*, 5958321. https://doi.org/10.1155/2017/5958321

[18] Bezak, E., Marcu, L., & Penfold, S. (2012). Computational and mathematical modeling of tumor kinetics and response to radiation and chemotherapy. *Computational and mathematical methods in medicine*, *2012*, 702675. https://doi.org/10.1155/2012/702675

[19] Scianna, M., Preziosi, L., & Wolf, K. (2013). A Cellular Potts Model simulating cell migration on and in matrix environments. *Mathematical biosciences and engineering : MBE*, *10*(1), 235–261. https://doi.org/10.3934/mbe.2013.10.235

[20] Voss-Böhme A. (2012). Multi-scale modeling in morphogenesis: a critical analysis of the cellular Potts model. *PloS one*, *7*(9), e42852. https://doi.org/10.1371/journal.pone.0042852

[21] Szabó, A., & Merks, R. M. (2013). Cellular potts modeling of tumor growth, tumor invasion, and tumor evolution. *Frontiers in oncology*, *3*, 87. https://doi.org/10.3389/fonc.2013.00087

[22] [Online]. Available: https://artistoo.net/explorables/Explorable-CPM.html. [Accessed 30 4 2023].

[23] Saxena, K., Jolly, M. K., & Balamurugan, K. (2020). Hypoxia, partial EMT and collective migration: Emerging culprits in metastasis. *Translational oncology*, *13*(11), 100845. https://doi.org/10.1016/j.tranon.2020.100845

[24] Ben-Salem, S., Venkadakrishnan, V. B., & Heemers, H. V. (2021). Novel insights in cell cycle dysregulation during prostate cancer progression. *Endocrine-related cancer*, *28*(6), R141–R155. https://doi.org/10.1530/ERC-20-0517

[25] Priya N. Werahera, L. Michael Glode, Francisco G. La Rosa, M. Scott Lucia, E. David Crawford, Kenneth Easterday, Holly T. Sullivan, Rameshwar S. Sidhu, Elizabeth Genova, Tammy Hedlund, "Proliferative Tumor Doubling Times of Prostatic Carcinoma", Prostate Cancer, vol. 2011, Article ID 301850, 7 pages, 2011. https://doi.org/10.1155/2011/301850

[26] Schmid, H. P., McNeal, J. E., & Stamey, T. A. (1993). Clinical observations on the doubling time of prostate cancer. European urology, 23 Suppl 2, 60–63. https://doi.org/10.1159/000474708

[27] Shin Egawa and others, Impact of Life Expectancy and Tumor Doubling Time on the Clinical Significance of Prostate Cancer in Japan, *Japanese Journal of Clinical Oncology*, Volume 27, Issue 6, December 1997, Pages 394–400, https://doi.org/10.1093/jjco/27.6.394